Combined Puncture and Cutting of Soft-Coated Fabrics by a Pointed Blade: Energy, Force, and Stress Failure Criteria

Abstract

Soft-coated fabrics are widely used in engineering and protective applications. Puncture cutting by sharp-tipped objects is one of the most common failure modes of protective gloves made of coated fabrics. In order to investigate the puncture-cutting process of soft-coated fabrics, we studied the mechanisms and mechanics of pointed-blade insertion into specimens cut out from four protective gloves. Experimental and analytical analyses showed that total energy and critical puncture-cutting force calculated analytically are both able to predict the puncture-cutting resistance of soft-coated fabrics measured experimentally. Total energy is obtained from the relationship between the puncture-cutting work and the created fracture area, while critical force is given by two analytical models developed in work with soft elastomeric membranes. The components of the critical puncture-cutting force are predicted analytically and then used to calculate the compressive and shear loading stress components based on the contact surface between the pointed blade tip and material. Since there is a linear relationship between the compressive stress component and shear stress component, a modified linear strength criterion is proposed for puncture cutting of soft-coated fabrics by a pointed blade. Our stress-based criterion connects the shear strength (in the 45° direction) and biaxial strengths (in the course direction, 0°, and wale direction, 90°) to both compressive and shear loading stresses. The analytical and experimental results are consistent. This investigation can be used as a guideline to evaluate the puncture cutting of soft-coated fabrics using an energy-based criterion, critical force-based criterion or stress-based criterion.

Keywords: puncture cutting, soft-coated fabrics, failure, criterion, stress

1. Introduction

Soft-coated fabrics consist of two different materials: (1) strong, tough, stiff fabrics with high elastic modulus and (2) synthetic elastomers. A good combination of two such materials has properties not available in a single material [1]. Soft-coated fabrics are widely used in protective equipment, such as protective gloves. The common architecture of protective gloves usually consists of a knitted fabric coated with a soft elastomeric material. The combination of stiff and soft materials results in very strong, very tough composite materials [2].

Workers in occupations such as metalworking, food processing and industrial papermaking commonly wear protective gloves of this kind, as they are exposed to various cut and puncture hazards. Failure of soft-coated fabric caused by an indenter or blade has not much been investigated. Some researchers have tested the puncture resistance of coated fabrics using a rounded probe [3,4] or a flat-tipped cylindrical probe [5]. Specific puncture mechanisms such as fiber stretching, breaking and delamination have been considered the main contributors to the puncture of an uncoated material by a rounded probe [6], but Hassim et al. showed that all these mechanisms become insignificant in the puncturing of coated fabrics, due to the effect of the coating layer. Furthermore, they showed that the coating layer restricts the deformation of the specimen. They observed a circular deformation on the front face of the specimen, but only a small deformation on the back face. Although there is very little information in the literature on the puncture and cutting mechanics of soft-coated fabrics, the failure mechanisms and mechanics of fabrics in general have been widely investigated [6,7]. In the quasi-static puncture of high-strength polyester yarns, the indenter experiences yarn slippage during penetration due to the contact pressure [6], whereas the slice-push cutting of woven and knitted fabrics by a blade shows that two types of friction control the critical cutting force: a macroscopic friction on both sides of the blade and a sliding friction on the cutting edge of the blade [7]. Vu Thi et al. applied the same cutting mechanics to fabric materials and elastomeric membranes to investigate the force state. They showed that the critical cutting force is a result of the pushing force and the slice friction force exerted by the cutting edge of the blade. In this case, the critical force was related to the local effective shear strength of the interface.

To our knowledge, no analytical study has considered the puncture-cutting mechanisms that occur during the insertion of an indenter into soft-coated fabrics. However, in an effort to better understand this combined pushing and shear loading, recent studies have focused on modeling the puncture and/or cutting of soft isotropic solids. The failure behavior of isotropic material has been determined in terms of critical force [8,9,10], energy [11] or stress [12,13,14]. Triki and Gauvin showed that the combined puncture and cutting of soft elastomeric membranes by a pointed blade results from a combined loading of the compressive stress component (σ) and the shear stress component (τ) at the cut edge of the material [14]. They described the relationship between σ and τ using a linear stress-based criterion to predict the failure strength corresponding to pointed-blade insertion into soft isotropic membranes (neoprene rubber) [14]. On the other hand, in the case of orthotropic materials, such as soft-coated fabrics, subjected to complex loading, many classical strength criteria, including the Yingying criterion [2], Tsai-Hill criterion [15,16], Yeh-Stratton criterion [17], Hashin criterion [18] and Norris criterion [19], have been used to predict the tensile strength of materials. All these criteria are always composed of applied stresses, shear strength and tensile strength along the principal axes of the fabric structure.

Furthermore, the tearing of soft-coated fabrics was also modeled by Triki et al. [20], who proposed an energetic approach based on the Griffith theory [21].

The main objective of the work described here was to model the combined puncture cutting of soft-coated fabrics with a view to proposing a fracture criterion. We extended our analytical analysis of puncture cutting of soft isotropic materials in [14] to soft orthotropic materials, evaluating puncture-cutting resistance through force measurement and energy calculation. Uniaxial tensile tests were carried out, as well, to measure the mechanical properties of materials that could be involved during puncture-cutting tests. Then, we modeled the critical puncture-cutting force using the stress state analysis that had been developed for pointed-blade insertion into soft elastomeric materials. Finally, we came up with a stress-based criterion derived from our experimental results.

2. Force state corresponding to pointed-blade insertion into soft-coated fabrics

In our recent paper on the puncture cutting of soft elastomeric membranes by a pointed blade [14], we analyzed the force field at the cut edge of the material (Figure 1). In that case, the force state at the cut edge is a combined loading of pushing and shear forces, and the material failure always occurs as the result of two applied forces: the pushing force component (F_P) in the z-direction (e_z) and the shear force component (F_C) in the x-direction (e_x).

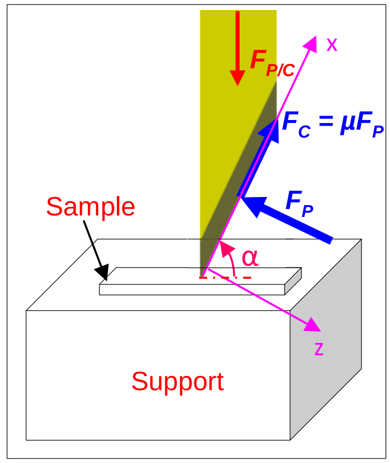

Figure 1. Combined puncture-cutting test: Force state analysis and relationship between puncture and cutting force components.

Furthermore, stress state analysis makes it possible to define the stresses involved in the pointed-blade insertion into the elastomeric membrane. Building on the work of Deibel et al. [9], Triki and Gauvin have shown that the stress state is governed by contact pressure (p) from the pointed blade in the normal direction of the created fracture surface [14]. Hence, both force components, F_P and F_C, have been expressed as

$$\begin{cases} F_P = 2A(\{S\})^T\{e_z\} = u_h u_v p \begin{pmatrix} \dfrac{\mu}{\sqrt{1+\zeta^2}} \\ 1 \\ \dfrac{\mu\zeta}{\sqrt{1+\zeta^2}} \end{pmatrix} \begin{pmatrix} 0 \\ 0 \\ 1 \end{pmatrix} = u_h u_v p \dfrac{\mu\zeta}{\sqrt{1+\zeta^2}} & (1) \\ F_C = 2A(\{S\})^T\{e_x\} = u_h u_v p \begin{pmatrix} \dfrac{\mu}{\sqrt{1+\zeta^2}} \\ 1 \\ \dfrac{\mu\zeta}{\sqrt{1+\zeta^2}} \end{pmatrix} \begin{pmatrix} 1 \\ 0 \\ 0 \end{pmatrix} = u_h u_v p \dfrac{\mu}{\sqrt{1+\zeta^2}} & (2) \\ with & \\ p = \dfrac{K_C}{\sqrt{c_I^2 L + c_{II}^2 L \dfrac{\mu^2\zeta^2}{1+\zeta^2} + c_{III}^2 L(1+\nu)\left(\dfrac{L}{t}\right)^2 \dfrac{\mu^2}{1+\zeta^2}}} & (3) \end{cases}$$

where A is the created fracture area; u_v is the vertical depth penetration and u_h is the horizontal cutting length; c_I, c_{II} and c_{III} are fitting parameters; μ is the friction coefficient in the cutting edge; ζ is the puncture-cut ratio ($\zeta = \tan\alpha$); L is the contact length; t is the material thickness; ν is the Poisson's ratio; and Kc is the critical stress intensity factor that can also be given as

$$K_C = \sqrt{EG_C} \qquad (4)$$

where E is the Young's modulus and G_C is the fracture toughness of the material.

To estimate the pressure, p, Deibel et al. [9] found that the three stress intensity factors could be calculated as

$$K_I = c_I p\sqrt{L} \qquad (5)$$

$$K_{II} = c_{II}\tau_{yz}\sqrt{L} \qquad (6)$$

$$K_{III} = c_{III}\tau_{yx}\frac{L}{t} \qquad (7)$$

where K_I, K_{II} and K_{III} are the stress intensity factors and τ_{yx} and τ_{yz} are the shear stresses acting at the cut edge of material [14].

As shown in Figure 1, the critical puncture-cutting force, $F_{P/C}$, was predicted from the above force components as

$$F_{P/C} = \sqrt{F_P^2 + F_C^2} \tag{8}$$

Moreover, using an energy-based approach, Triki and Gauvin also predicted, in [14], the value of $F_{P/C}$ as

$$F_{P/C} = \frac{G_{Total}\, t}{2\left[1+\zeta^2\right]^{1/2}} \tag{9}$$

where G_{Total} is the total puncture-cutting energy applied by a pointed blade.

In order to further examine the rationale behind our two models (Eqs. (8) and (9)) and to achieve an overall understanding of the main role of the pushing and shear forces, we extended these two models to the puncture cutting of soft-coated fabrics. To this end, we performed experimental tests on soft-coated fabrics and measured the total puncture-cutting energy using Poisson's ratio and Young's modulus as required in Eq. (3).

3. Material and experimental tests

3.1. Material

Four commercially available protective gloves made of a knitted fabric with rubber-dipped palms were used. The coating material and fabric construction are listed in Table 1. The specimens for the mechanical tests were cut out from the palms of the gloves.

Table 1. Material composition and fabric construction of protective gloves studied.

Protective gloves	Materials		t (mm)
	Coating	Liner	
A: HyFlex® 11-900 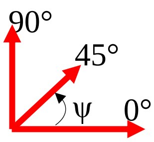 	Nitrile rubber	Knitted nylon	1
B: 80-813 PowerFlex 	Neoprene foam rubber	Knitted Kevlar®	1.3
C: ActivArmr® 97-100 	Neoprene rubber and nitrile rubber	Knitted Kevlar®, nylon, polyester and spandex	1.1
D: Superior Glove S13SXPU 	Polyurethane rubber	Knitted Dyneema®	1.3

3.2. Combined puncture-cutting test

The materials' puncture-cutting performance was measured by driving a pointed blade into the specimens. Each specimen was positioned on a soft neoprene rubber support (25 mm thick and 42 Shore A) coated with a silver/silver chloride layer (Ag/AgCl ink, Sigma-Aldrich, U.S.A.) as a conductive substrate (Figure 2a). A pointed blade was fixed to the crosshead of a universal testing machine (ADMET Inc., Norwood, MA) equipped with a 25 lb load cell. The puncture-cutting test consists in lowering the pointed blade into the specimen at a crosshead speed of 30 mm/min. Pointed blade displacement and force were recorded (Figure 2b). The conductive layer of Ag/AgCl was coupled with the blade to close an open circuit that detects the full penetration of the blade through the specimen, which occurs as soon as the blade tip comes into contact with the Ag/AgCl layer. The critical puncture-cutting force required to puncture and cut a soft-coated fabric corresponds to the force measured at the full penetration of the pointed blade. The critical force and total puncture-cutting work (U_{Total}) were obtained for three specimens (i.e., three replicates) of each glove material punctured by a pointed blade at various cutting-edge angles ($20^o \leq \alpha \leq 80^o$). The fracture surface area (A) was estimated from the inserted part of the pointed blade shape at full penetration and is given as

$$A = t^2/2tan\alpha \tag{10}$$

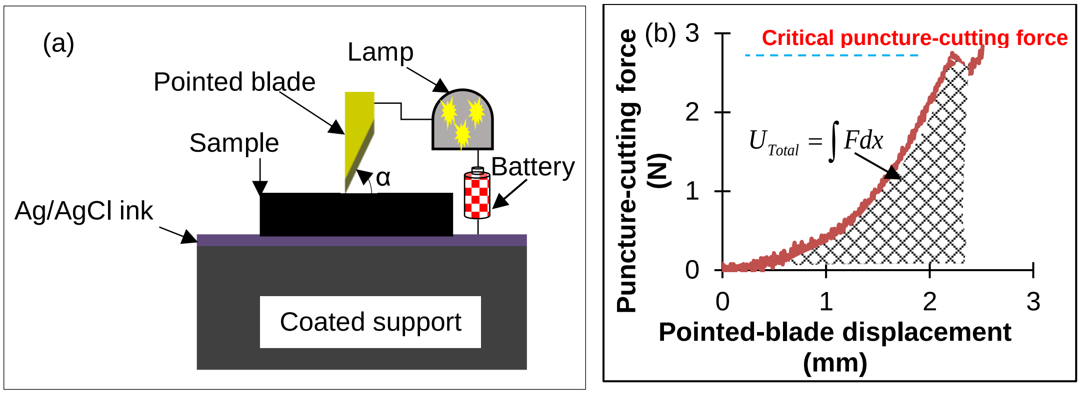

Figure 2. (a) Experimental setup of puncture-cutting test and (b) puncture-cutting force vs. pointed-blade displacement curve for soft-coated fabric specimen.

3.3. Uniaxial tensile test

Uniaxial tests were carried out to measure the material's tensile strength and Young's modulus. Specimens measuring 200 mm × 25 mm were cut out from the palms of protective gloves in three off-axial directions: the wale direction ($\psi = 90°$), course direction ($\psi = 0°$) and shear direction ($\psi = 45°$) (see Table 1). The specimens were clamped in the opposing clamping jaws of an MTS-Alliance tensile machine equipped with an automated data acquisition system (Figure 3a) and the two ends were pulled apart at a constant crosshead speed of 500 mm/min until the specimen ruptured. For each direction, three specimens were tested, and the strain-stress curve was recorded (Figure 3b).

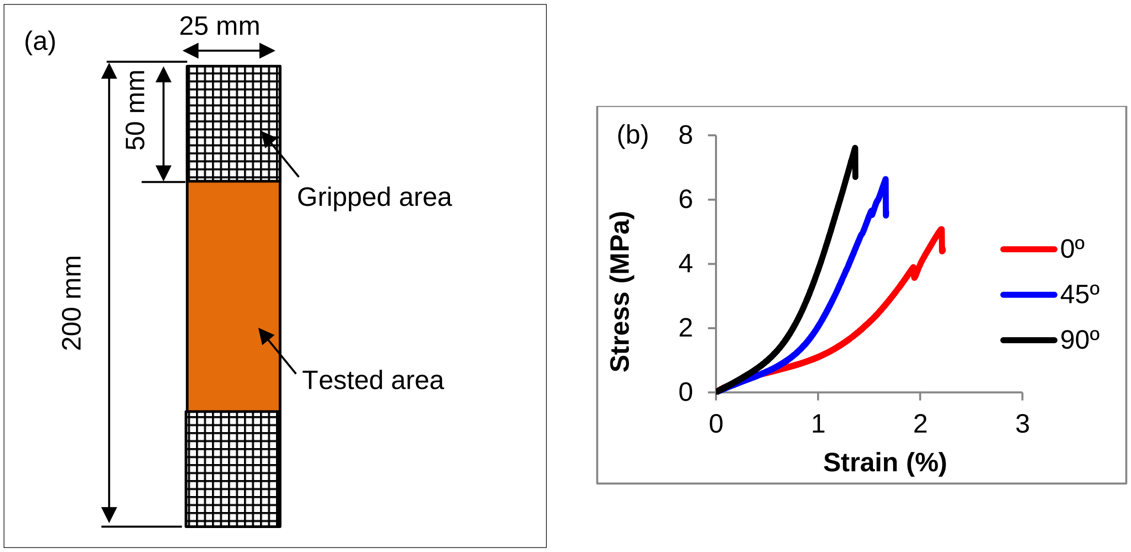

Figure 3. Uniaxial tensile test: (a) Dimension of tensile test specimen and (b) typical curves of stress vs. strain obtained in three directions.

3.4. Poisson's ratio test

In order to measure the Poisson's ratio, three rectangles (ABCD, CDEF and ABEF) were selected in the 200 mm × 25 mm specimen, which was loaded at 500 mm/min in uniaxial stress (Figure 4a). Many digital photos of the loaded specimen were recorded at successive strain values. The photos were then imported into ImagJ to estimate the displacement in length (Δl) and width (Δb) of all three rectangles (Figure 4b). Extension (ε_i) and contraction (s_i) were calculated at various steps of deformation, i = 5%, 10%, 50%, 100%, etc., using Eqs. (11) and (12), respectively.

$$\varepsilon_i = \frac{\Delta l_i}{l_0}.100\% \tag{11}$$

$$s_i = \frac{\Delta b_i}{b_0}.100\% \tag{12}$$

The average of the transverse strains ($\bar{s}_i$), corresponding to the contraction of AB, CD and EF, and axial strains ($\bar{\varepsilon}_i$), corresponding to the extension of AC, CE and AE, were used to obtain the Poisson's ratio of the coated fabric at a deformation *i* as

$$\nu_i = -\frac{\bar{s}_i}{\bar{\varepsilon}_i} \tag{13}$$

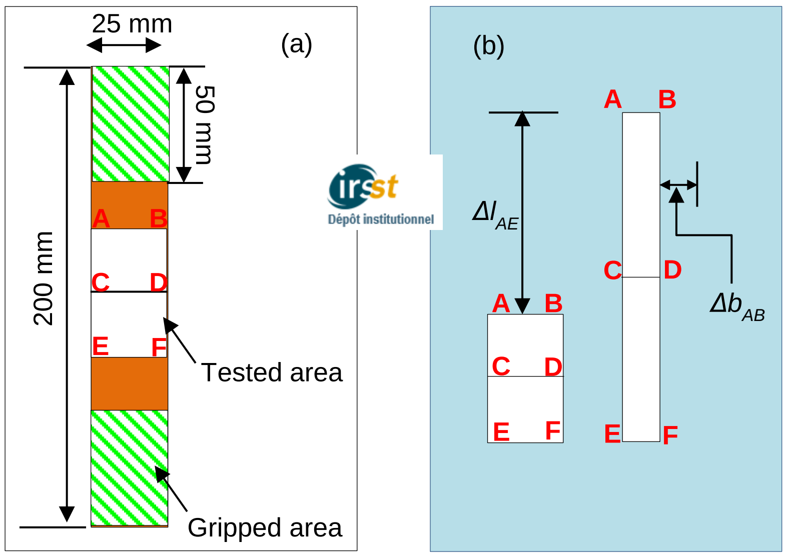

Figure 4. Uniaxial tensile test of coated fabric: (a) Undeformed specimen and b) axial displacement (Δl) and lateral displacement (Δb) of tested specimen.

4. Results and discussion

4.1. Puncture-cutting mechanisms of soft-coated fabrics

To understand the failure of soft-coated fabrics caused by a pointed blade (Figures 5a and b), it was necessary to investigate the force-pointed blade displacement curves obtained from the three replicates (Figure 5c). As loading begins, a small material deformation is enough to initiate crack nucleation, due to the blade's acute tip and its cutting edge (Figure 5b). As shown in Figure 5c, the nucleation process required a small applied force ($\leq$ 0.5 N). The material shows low elastic deformation resistance. Once the pointed blade smoothly penetrates the specimen (Figures 5d and e), the applied force gradually increases until it reaches a maximum value, the critical puncture-cutting force, $F_{P/C}$ (Figure 5b). $F_{P/C}$ corresponds to the full penetration of the pointed blade into the specimen. Furthermore, during the pointed-blade insertion, the elastic deformation resistance of the material is found to increase remarkably. This trend could be associated with the friction between the pointed blade and material, which does not happen during crack nucleation. In the linear part of these curves, the measured force is therefore a result of fracture and friction mechanisms. Triki et al. found that the puncture-cutting energy of soft elastomeric membranes by a pointed blade includes a friction contribution of over 60% [22]. At the critical puncture-cutting force, the material deformation reaches a maximum value and the pointed blade penetrates all the way through the specimen. Deep penetration by the pointed blade involves a radial expansion of the material, which is highly dependent on the cutting-edge angle (α) (Figures 5e and f). Insertion of a pointed blade having a small α gives rise to high radial material deformation. The curves given as an example in Figure 5c show that the pointed blade penetrates the soft-coated fabric smoothly and gradually, and that behavior of the material is uniform until full penetration by the pointed blade is achieved. It thus appears that the knitted fabric on the underside of the specimen does not contribute to the puncture-cutting process.

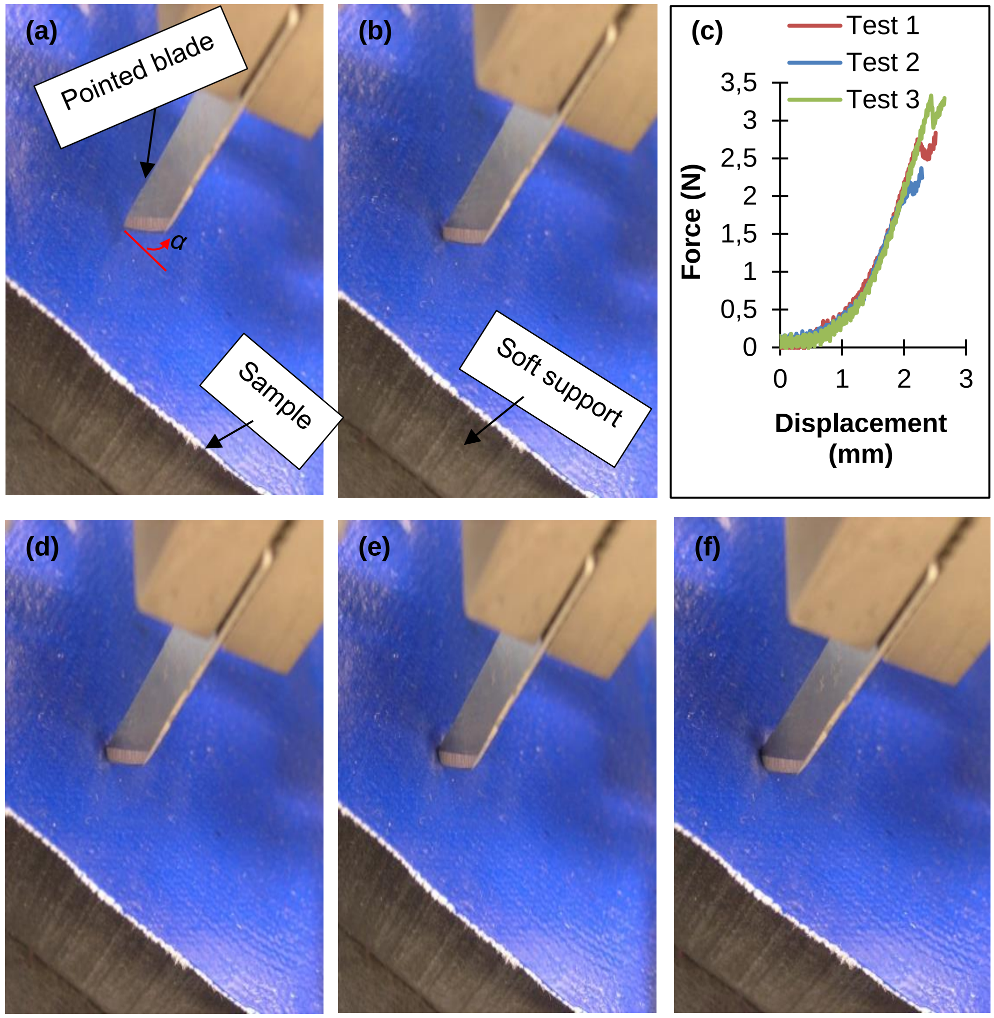

Figure 5. Puncture-cutting test of soft-coated fabric by pointed blade: (a) Unpunctured specimen, (b) crack nucleation step, (c) force-blade displacement curve recorded during insertion process for three replicates, and (d), (e) and (f) typical penetration steps.

4.2. Energy-based approach of combined puncture and cutting test

In this section, total puncture-cutting energy, G_{Total}, was calculated using a procedure outlined in our previous articles [11,14]. According to this procedure, G_{Total} is given by

$$G_{Total} = -\frac{\partial U_{Total}}{\partial A} \approx \frac{\Delta U_{Total}}{\Delta A} \quad (14)$$

where ΔU_{Total} is the change in the total puncture-cutting work corresponding to the change in fracture surface area, ΔA, which was measured for each α as detailed in [14].

The puncture-cutting tests on the four protective gloves were carried out for various cutting-edge angles. Figure 6 displays the variation of U_{Total} as a function of the created surface of the puncture-cutting crack area (A) for the four protective gloves. For each glove, the puncture-cutting work appears to be linearly proportional to the fracture surface area. This linearity indicates that the proposed total puncture-cutting energy defined by Eq. (14) seems to be valid for those composite materials. G_{Total} is given by the slope of the regression line in Figure 6. It is important to note that the coefficient of variation in all experimental tests (puncture cutting and tensile tests) was less than 9%.

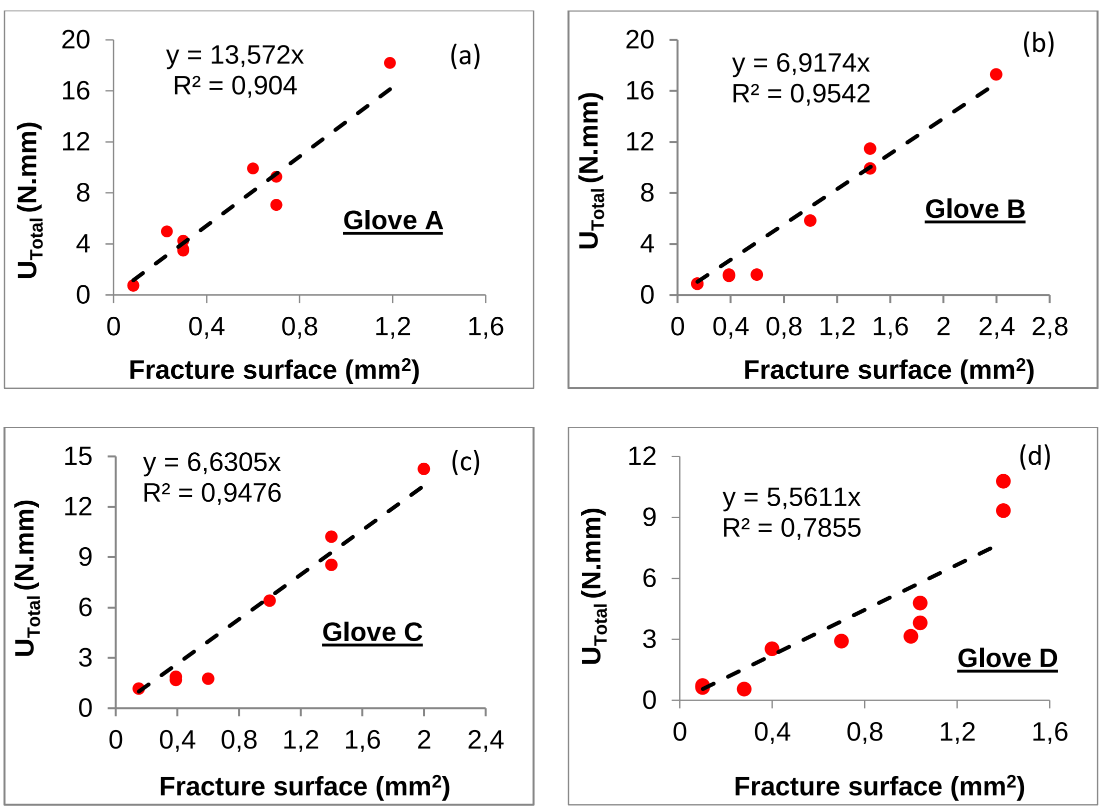

Figure 6. Variation of puncture-cutting work (U_{Total}) as a function of crack surface area (A) for (a) HyFlex® 11-900, (b) 80-813 PowerFlex, (c) ActivArmr® 97-100 and (d) Superior Glove S13SXPU.

4.3. Uniaxial and biaxial test results

Uniaxial tensile tests were conducted to measure the mechanical properties of soft-coated fabrics and then predict the biaxial tensile properties that may be involved during the insertion of a pointed-blade, such as tensile strength in the wale and course directions. After that, the values of these properties were used as described in section 4.4 to predict puncture-cutting behavior.

The values obtained for uniaxial tensile strength (σ_U), shear strength (S) and Young's modulus (E) are presented in Table 2. It can be seen in Figure 3b that E is almost the same for the three loading directions (0°, 45° and 90°).

Table 2. Values of tensile and shear strengths (σ_U and S) and Young's modulus (E) of four protective gloves in three off-axial directions.

	Protective gloves			
	A: 11-900	**B: 80-813**	**C: 97-100**	**D: S13SXPU**
Off-axial angle (°)	**σ_U (MPa)**			
0	5.05	15.03	7.22	12.64
90	7.5	14.87	7	23.05
S (MPa)				
45	6.6	9.23	7.03	10.4
E (MPa)				
0, 45 and 90	6.4	6.1	5.47	6.06

The experimental results for the four protective gloves given in Table 2 and Figure 6 reveal that there appears to be no correlation between G_{Total} and σ_U, S or E. For example, the gloves with high G_{Total} did not necessarily perform well in terms of uniaxial tensile properties. Hence, the uniaxial tensile test results in the three off-axial directions cannot predict the puncture-cutting behaviors of soft-coated fabrics. However, developing a relationship between these uniaxial tensile properties may predict the behavior of material during pointed-blade insertion, as has been done in the case of woven fabric subjected to complex loading [2].

Poisson's ratio is one of the fundamental properties of all structural materials, such as soft-coated fabrics. For that reason, we used it to predict the biaxial tensile properties and then puncture-cutting behaviors of soft-coated fabrics. The average values of Poisson's ratio were obtained for the three off-axial directions (three replicates each) at various stages of specimen deformation, illustrated in Figure 7. At the beginning of the uniaxial tensile test, more axial than lateral extension of the specimen is observed, due to the hyperelastic behavior of the coating material (Figure 7). The increase in the specimen's axial extension leads to a gradual increase in Poisson's ratio until maximum values are reached at an extension of around 100%. At that point, the coated fabrics show maximum lateral strain: the contraction of the specimen seems stable, while its extension progresses. Consequently, the Poisson's ratio value decreases. As shown in Figure 7, the Poisson's ratio-strain curve shows a similar tendency in the three off-axial directions tested for all four protective gloves. The maximum Poisson's ratio values presented in Table 3 were used as described in section 5.4 to predict the critical puncture-cutting force of soft-coated fabrics, as required in Eq. (8).

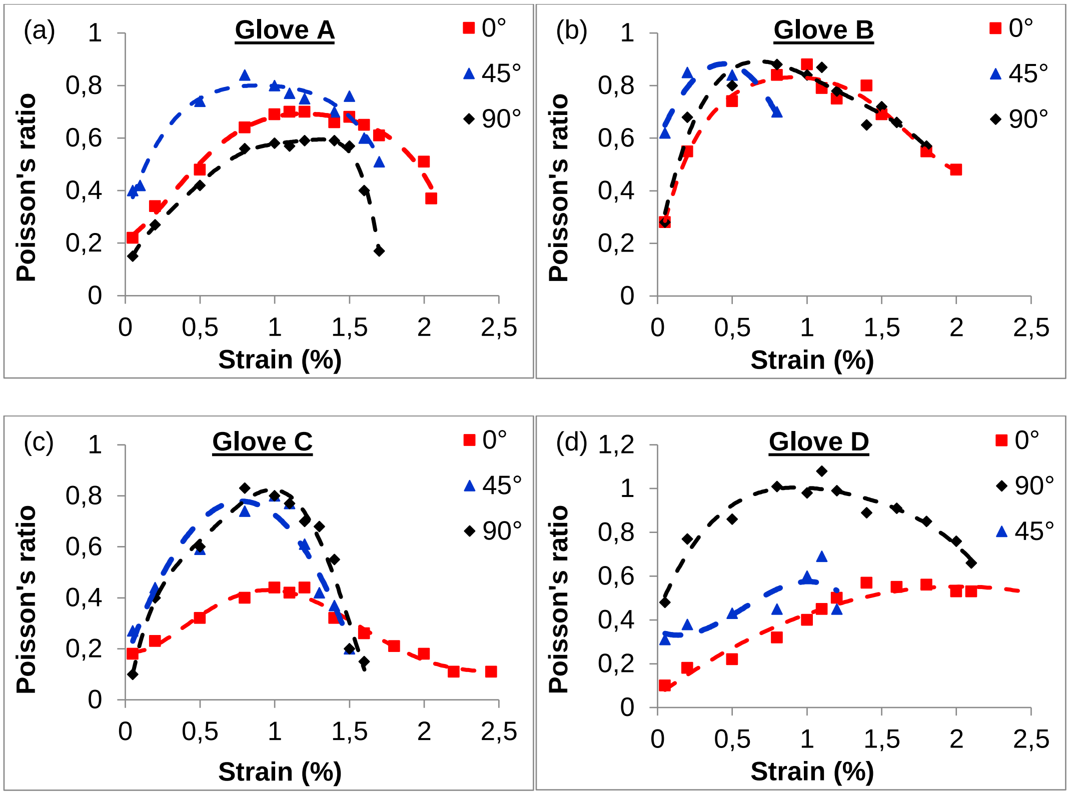

Figure 7. Typical curves of Poisson's ratio vs. strain obtained in three off-axial directions, 0°, 45° and 90°, for (a) HyFlex® 11-900, (b) 80-813 PowerFlex, (c) ActivArmr® 97-100 and (d) Superior Glove S13SXPU.

Table 3. Maximum Poisson's ratio values for four protective gloves obtained in three off-axial directions.

	Protective gloves			
	A: 11-900	**B: 80-813**	**C: 97-100**	**D: S13SXPU**
Off-axial angle (°)	ν_{max}			
0	0.68	0.84	0.42	0.57
45	0.84	0.84	0.8	0.69
90	0.58	0.98	0.97	1.01

The biaxial tensile strengths of soft-coated knitted fabric in the wale direction (σ_1, corresponding to 90°) and course direction (σ_2, corresponding to 0°) were predicted by means of the uniaxial tensile strength using equations proposed by Ambroziak [23] for coated woven fabric:

$$\sigma_1 = \frac{F_1(\varepsilon_1)}{1-\nu_{12}\nu_{21}}(\varepsilon_1 + \nu_{21}.\varepsilon_2) \tag{15}$$

$$\sigma_2 = \frac{F_2(\varepsilon_2)}{1-\nu_{12}\nu_{21}}(\varepsilon_2 + \nu_{12}.\varepsilon_1) \tag{16}$$

where F_1 (ε_1) and F_2 (ε_2) are respectively the wale and course longitudinal stiffnesses estimated on the basis of the uniaxial tensile test, and ν_{12} and ν_{21} are the Poisson's ratios. Using the results of Poisson's ratio illustrated in Table 3, Eqs. (15) and (16) allow us to plot typical strain-stress curves for those two directions (Figure 8), as detailed in [23]. The maximum values of the predicted biaxial tensile stress corresponding to the moment of a specimen's failure are collected in Table 4. As shown in Figure 8, no similarity is observed between the uniaxial data and predicted biaxial results. The predicted biaxial results were used as described in section 5.5 to develop a new fracture criterion.

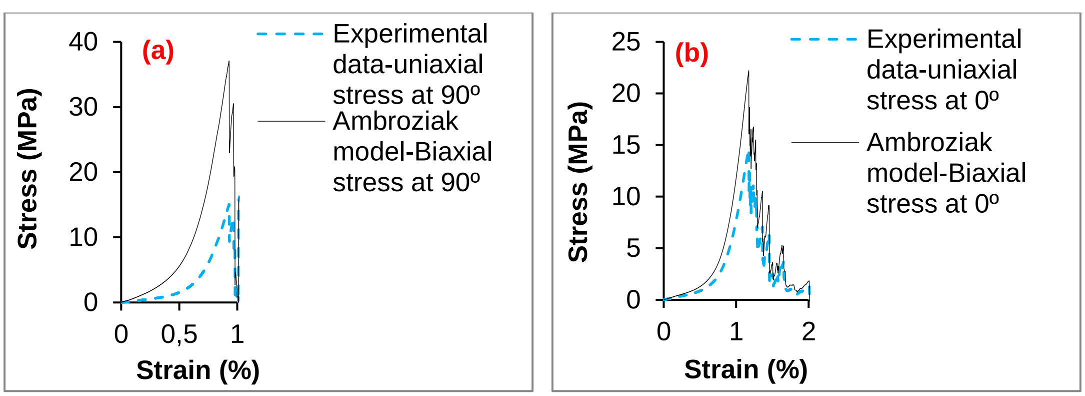

Figure 8. Typical predicted curves of stress vs strain of biaxial tensile test corresponding to (a) wale direction (90°) and (b) course direction (0°) obtained for PowerFlex 80-813.

Table 4. Values of biaxial tensile strength stress of four protective gloves obtained at two off-axial directions.

	Protective gloves			
	A: 11-900	**B: 80-813**	**C: 97-100**	**D: S13SXPU**
Off-axial angle (°)	**Biaxial tensile strength (MPa)**			
0	6.31	22.22	8.5	16.53
90	15.3	36.85	15.59	29.4

4.4. Force-based approach

In this section, we examine the two analytical models of critical puncture-cutting force, which were developed for soft elastomeric membranes and based on energetic analysis (Eq. (9)) [10] and stress analysis (Eq. (8)) [14]. In Eqs. (8) and (9), $F_{P/C}$ depends not only on total energy (Figure 6), Poisson's ratio (Table 3) and Young's modulus (Table 2), but also on fracture energy, G_C, (fracture toughness) and the three fitting parameters. As mentioned in section 5.2, it is assumed that the contribution of the fabric structure during the puncture-cutting test is negligible due to the blade's acute tip. Therefore, G_C can be estimated to be about 40% of G_{Total}, as it is the case for soft elastomeric materials reported by Triki et al. [11]. The same values of the fitting parameters ($c_I = 0.055$, $c_{II} = 0.55$ and $c_{III} = 0.8$) estimated for puncture cutting of soft elastomeric membrane were then used for soft-coated fabrics.

Figure 9 provides a graphical representation of the variation in critical puncture-cutting force as a function of cutting-edge angle, which was obtained from experimental data, and our two analytical models of the stress-based approach (Eq. (8)) and energy-based approach (Eq. (9)). Our results indicate that the two proposed models are good predictors of the puncture-cutting resistance of soft-coated fabrics by pointed blades.

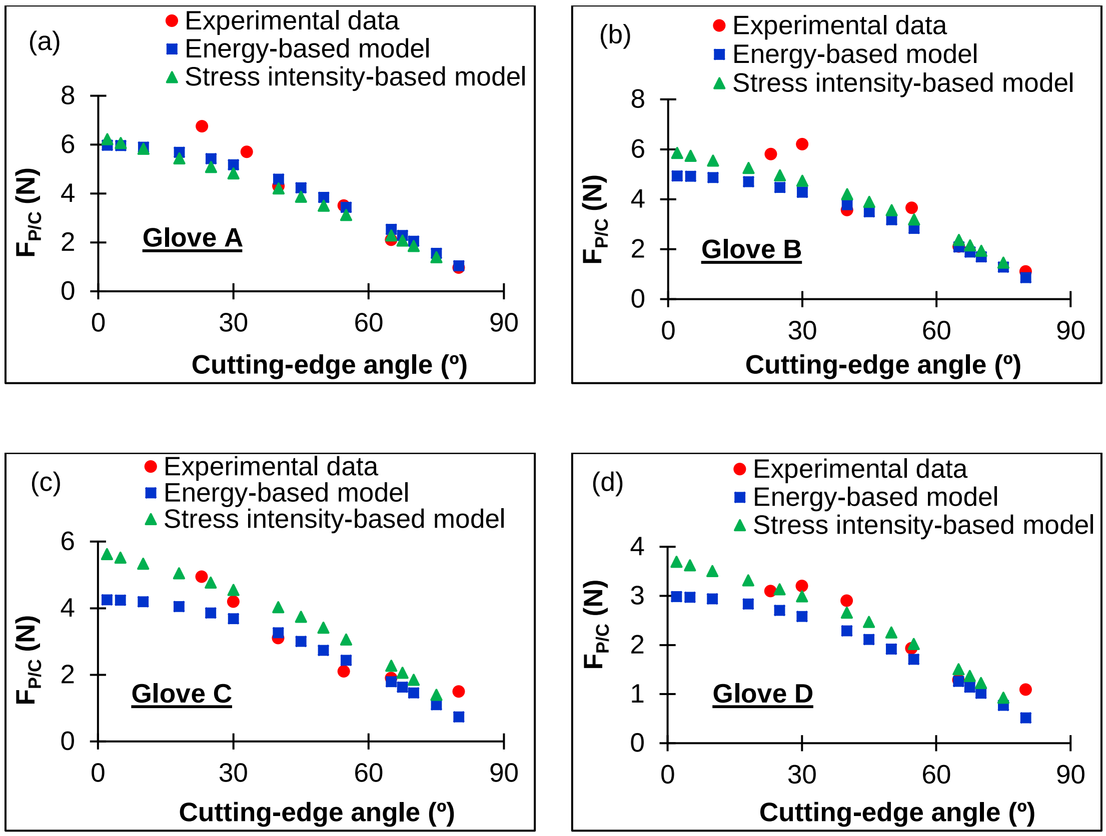

Figure 9. Comparison of predicted data (Eqs. (8) and (9)) and experimental data for four protective gloves, (a) HyFlex® 11-900, (b) 80-813 PowerFlex, (c) ActivArmr® 97-100, and (d) Superior Glove S13SXPU.

The decrease in critical puncture-cutting forces ($F_{P/C}$) with cutting-edge angle (α), seen in Figure 9, can be explained by studying how F_P and F_C values change with α. The influence of α can be clearly seen in the force profiles shown in Figure 10. For the four protective gloves of various thicknesses, the predicted profiles of the pushing force component (Eq. (1)) and shear force component (Eq. (2)) show the same characteristic behavior with the change in the cutting-edge angle. Our results show that pushing force decreases with cutting-edge angle, while shear force increases until it reaches a maximum (when $\alpha \approx 45°$) and then decreases. Although this shear force profile was unexpected, it is consistent with experimental data obtained by slicing soft gel by a wire [13].

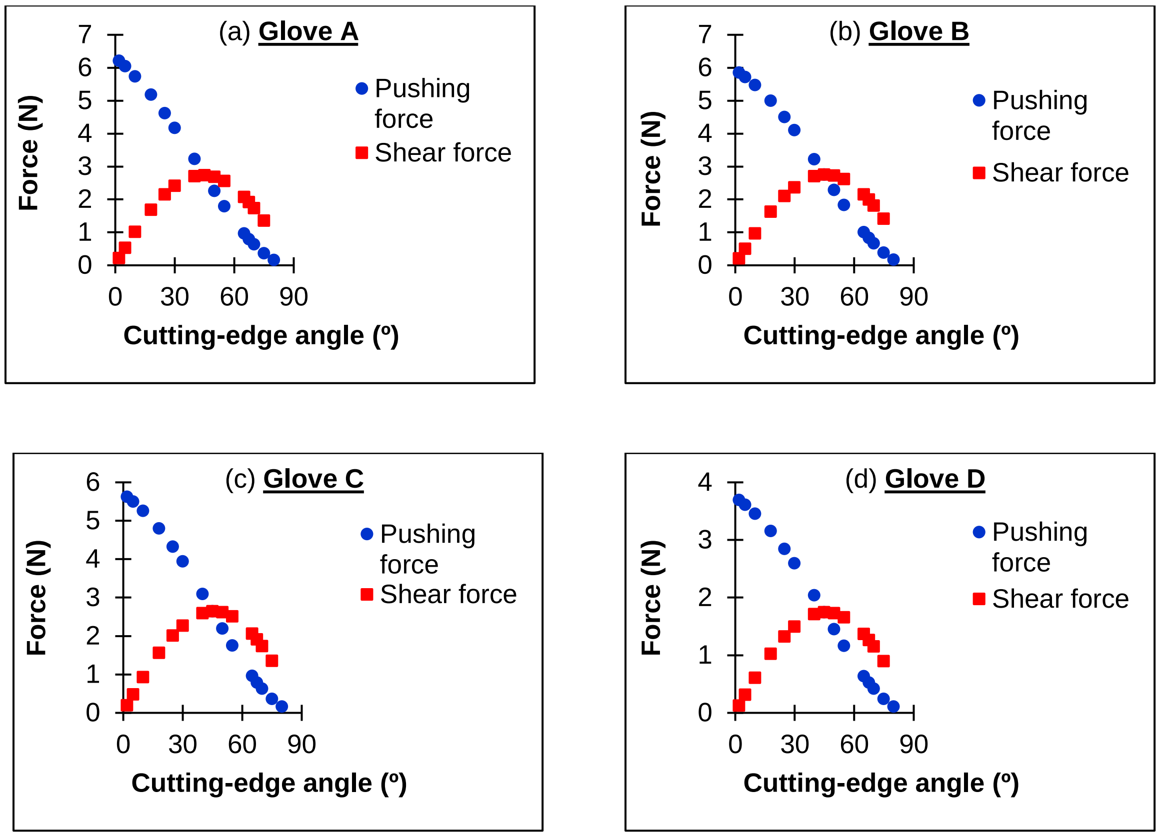

Figure 10. Typical curves of predicted pushing force (F_P) and shear force (F_C) as a function of cutting-edge angle for (a) HyFlex® 11-900, (b) 80-813 PowerFlex, (c) ActivArmr® 97-100 and (d) Superior Glove S13SXPU.

4.5. New stress-based failure criterion

In this section, we propose a linear stress-based criterion for pointed-blade insertion into soft-coated fabrics using the analysis developed for soft elastomeric membranes detailed in [14]. The compressive stress (σ) and shear stress (τ) acting at the cut edge of the material were calculated from F_P and F_S, respectively. As they established a linear relationship between σ and τ, Triki and Gauvin proposed a linear strength criterion for insertion of pointed blades into soft elastomeric membranes [14]. The blade's acute tip has a low coefficient of friction (μ << 1), so the effect of the fabric structure can be neglected in the puncture-cutting process. We therefore took our solution of the contact surface developed for pointed blades and elastomeric membranes and applied it here to soft-coated fabrics. In [14], we estimated the contact surface corresponding to the pushing force components as

$$A_{eff}^{pushing} = Kt^{m+1} \tag{17}$$

where K and m are constants to be determined, and t is the maximum deflection of the material by a pointed blade. The two parameters, K and m, were determined in the extreme puncture-cutting cases: $\alpha \rightarrow 0$ ($\tau \rightarrow 0$) and $\alpha \rightarrow 90$ ($\sigma \rightarrow 0$) [14].

The effective shear contact area, A_{eff}^{shear}, corresponding to the shear force was estimated in [14] as

$$A_{eff}^{shear} = \frac{t.e}{\tan\alpha} \tag{18}$$

where e is the contact width between the material and cutting edge, estimated using digital photo analysis. We applied a thin white layer of paint to the upper face of the specimen and waited for 5 to 10 minutes until the test surface was dry. After the pointed-blade had been inserted and retracted, a digital photo that included the fracture process zone was then recorded and analyzed in ImageJ in order to estimate the contact width, e (Figure 11).

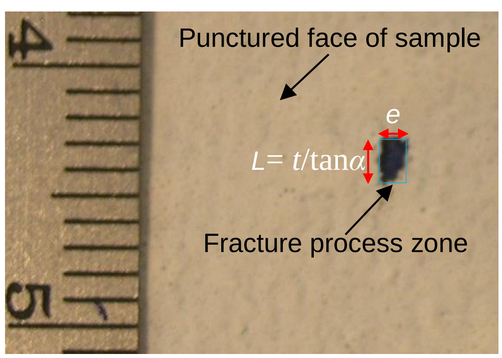

Figure 11. Digital photo of punctured specimen showing fracture process zone.

After calculating the contact areas from Eq. (17) and Eq. (18) and considering the pushing force and shear force, the compressive stress (σ) and shear stress (τ) components were calculated. Figure 12 shows the variation of σ and τ as a function of α. Interestingly, when α is small, the failure of the membrane is dominated by compressive stress, while at high α values, shear stress dominates; in other words, τ becomes maximum (Figure 12a). The results illustrate that puncture cutting of soft-coated fabrics involves a pushing/shear-dependent loading that indicates mixed failure modes [14]. The synergistic variation between the compressive stress component and shear stress component, at $0° < \alpha < 90°$, allows a linear relationship, σ-τ (Figure 12b).

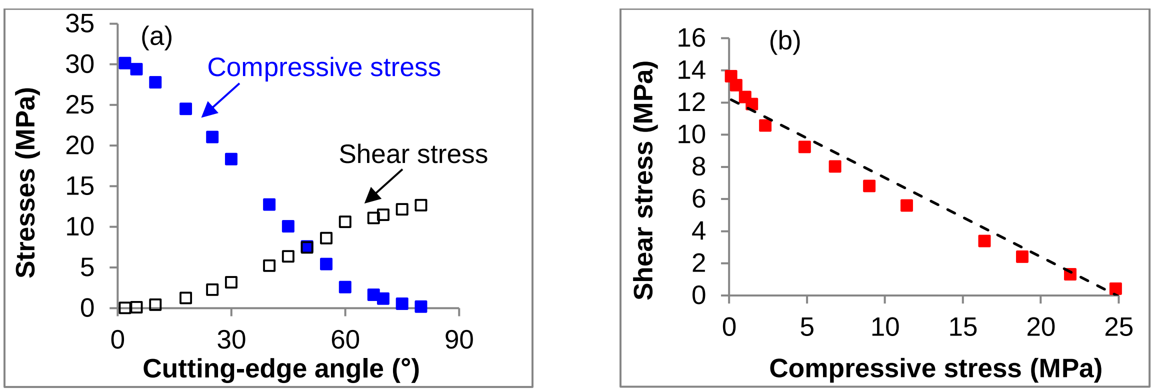

Figure 12. (a) Typical curve of applied stresses vs. cutting-edge angle and (b) typical curve of relationship between compressive stress component and shear stress component for soft-coated fabrics.

Due to the linearity between σ and τ discussed above, the linear strength criterion used in combined loading of soft elastomeric membranes [14] and composite materials [24,25] can be adopted here. Since the behavior of soft-coated fabrics is anisotropic, the linear strength criterion, σ-τ, is modified in order to take into account the material strengths corresponding to the wale direction (ψ = 90°), course direction (ψ = 0°) and shear direction (ψ = 45°). The new linear relationship is therefore described as

$$\frac{\tau}{S}+\frac{\sigma}{(X.Y)^{0.5}}=1 \tag{19}$$

where X, Y and S are the material strengths corresponding to the course, wale and shear directions, respectively.

By predicting X and Y (Table 4) and measuring S (Table 2), it is possible to plot the predicted shear stress as a function of compressive stress (Figure 13). As shown in Figure 13, the proposed criterion describes well the fracture behavior generated in combined loading of compressive and shear stresses that occurs at various cutting-edge angles.

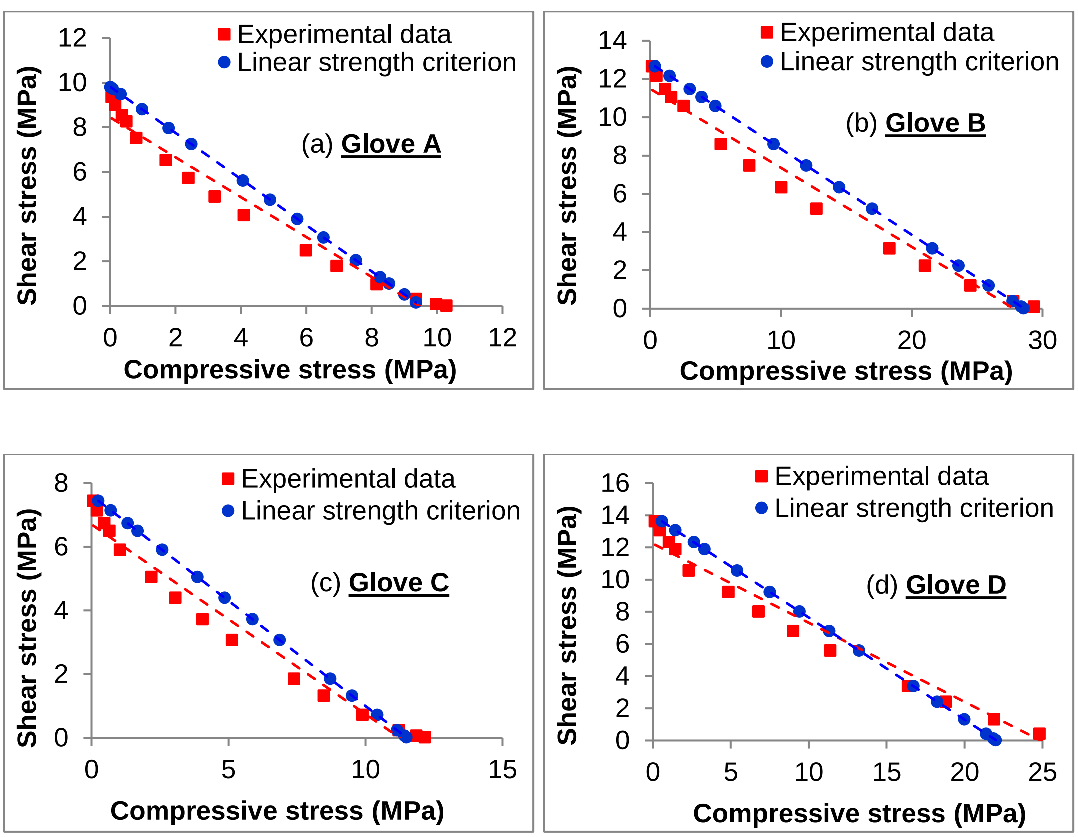

Figure 13. Comparison between experimental data and prediction data from linear strength criterion of (a) HyFlex® 11-900, (b) 80-813 PowerFlex, (c) ActivArmr® 97-100 and (d) Superior Glove S13SXPU.

5. Conclusions

Experimental and modeling investigations were conducted with a view to proposing a stress-based criterion for the puncture cutting of soft-coated fabric by a pointed blade. We focused on the mechanisms and mechanics of the puncture-cutting process. The experimental results show that the process of inserting a pointed blade into a soft-coated fabric involves the material's stiffness and toughness, as well as the friction between pointed blade and material. However, due to its structural design, the fabric support on the back of the specimen does not make any contribution during the insertion process. We also found that the puncture-cutting process generates a high local material deformation, which involves the mechanical properties in the three off-axial directions: wale, course and shear. Thus, modeling of the stress field in pointed-blade insertion into soft-coated fabrics should take into account those properties, and particularly biaxial tensile strength. For that reason, uniaxial tensile strength, Poisson's ratio, Young's modulus and material deformation were measured to predict the biaxial strengths in the course and wale directions. Two analytical models of energy and critical force corresponding to puncture cutting of soft elastomeric membranes were used successfully to develop a new stress-based criterion for puncture-cutting resistance of soft-coated fabrics. In the analytical model, the critical force ($F_{P/C}$) is generated by two force components: pushing and shear. From these two forces, the compressive stress component (σ) and shear stress component (τ) are calculated using analytical and experimental results involving the contact surface between the material and the pointed blade. Because there is a linear relationship between σ and τ, a modified linear strength criterion was derived from the stress criterion that had been developed for soft elastomeric materials. The predicted and experimental values were consistent, suggesting that puncture-cut resistance of protective materials can be evaluated by measuring the stresses. The results also showed that the biaxial strengths, which involve the deformation and rigidity of the material, have an important effect on the puncture-cutting process.

6. Acknowledgements

The authors would like to thank the Institut de recherche Robert-Sauvé en santé et en sécurité du travail (IRSST) for its financial support of this work.

7. References

1. Ashby MF. Hybrids to fill holes in material property space. *Philos Mag* 2005; 85: 3235–3257. DOI:10.1080/14786430500079892.

2. Yingying Z, Xiaoguang S, Qilin Z et al. Fracture failure analysis and strength criterion for PTFE-coated woven fabrics. *J Compos Mater 2015*; 49(12): 1409–1421. DOI: 10.1177/0021998314534706.

3. Hassim N, Ahmad MR, Ahmad WYW et al. Puncture resistance of natural rubber latex unidirectional coated fabrics. *J Ind Text* 2011; 42(2): 118–131.

4. Ahmad MR, Hassim N, Ahmad WYW et al. Quasi-static puncture resistance of unidirectional coated fabric. In: *2012 IEEE Symposium on Business, Engineering and Industrial Applications*, Bandung, Indonesia, September 23–26, 2012, pp. 468–472.

5. Wang P, Zhang Y and Sun B. Tear and puncture behavior of flexible composites. In: *18th International Conference on Composite Materials*, Jeju Island, Korea, August 21–26, 2011, pp. 21–26.

6. Wang QS, Sun RJ, Tian X et al. Quasi-static puncture resistance behaviors of high-strength polyester fabric for soft body armor. *Res Phy* 2016; 6: 554–560. DOI: 10.1016/j.rinp.2016.08.018.

7. Vu Thi BN, Vu-Khanh T and Lara J. Mechanics and mechanism of cut resistance of protective materials. *Theor Appl Fract Mech* 2009; 52: 7–13.

8. Atkins AG, Xu X and Jeronimidis G. Cutting, by 'pressing and slicing' of thin floppy slices of materials illustrated by experiments on cheddar cheese and salami. *J Mater Sci* 2004; 39: 2761–2766. DOI: 10.1023/B:JMSC.0000021451.17182.86.

9. Deibel K, Raemy C and Wegener K. Modeling slice-push cutting forces of a sheet stack based on fracture mechanics. *Eng Fract Mech* 2014; 124-125: 234—247. DOI: 10.1016/j.engfracmech.2014.04.029.

10. Triki E and Gauvin C. Analytical and experimental investigation of puncture-cut resistance of soft membranes. Submitted to *Mech Mater* 2018.

11. Triki E, Nguyen-Tri P, Gauvin C et al. Combined puncture and cutting of elastomer membranes: A fracture energy approach. *J Appl Polym Sci* 2017; 134: 44945. DOI: 10.1002/app.44945.

12. McCarthy CT, Annaidh A and Gilchrist MD. On the sharpness of straight edge blades in cutting soft solids: Part II – Analysis of blade geometry. *Eng Fract Mech* 2010; 77(3): 437–451.

13. Reyssat E, Tallinen T, Le Merrer M et al. Slicing softly with shear. *Phys Rev Lett* 2012; 109: 244301.

14. Triki E and Gauvin C. Stress state analysis in combined puncture-cutting of soft materials and tension-shear fracture criterion. Submitted to *Eng Fail Anal* 2018.

15. Hill R. *The mathematical theory of plasticity*. Oxford: Oxford University Press, 1950.

16. Tsai SW. *Strength & life of composites*. Composites Design Group, Stanford, 2008.

17. Yeh HY and Kim CH. The Yeh-Stratton criterion for composite materials. *J Compos Mater* 1994; 28: 926–939.

18. Hashin Z. Failure criteria for unidirectional fiber composites. *J Appl Mech* 1980; 47: 329–334.

19. Norris CB. *Strength of orthotropic materials subjected to combined stresses.* Misc. Pub FPL-1816. Madison, WI: U.S. Dept. of Agriculture, Forest Service, Forest Products Laboratory, 1962.

20. Triki E, Arrieta C, Boukehili H et al. Tear behavior of polyester-based coated textiles after thermo-oxidative aging. *Polym Compos* 2012; 33(6): 1007–1017. DOI : 10.1002/pc.22227

21. Griffith AA. Phenomena of rupture and flow in solids. *Philos Trans R Soc London, Ser.A* 1921; 221(582–593): 163–198. DOI: 10.1098/rsta.1921.0006.

22. Triki E, Nguyen-Tri P, Azaiez M et al. Combined puncture/cutting of elastomer membranes by pointed blades: Characterization of mechanisms. *J Appl Polym Sci* 2015; 132(26), 42150. DOI: 10.1002/app.42150.

23. Ambroziak A. Mechanical properties of polyester coated fabric subjected to biaxial loading. *J Mater Civ Eng* 2015; 27(11): 04015012. DOI: 10.1061/(ASCE)MT.1943-5533.0001265.

24. Kintscher M, Kärger L, Wetzel A et al. Stiffness and failure behaviour of folded sandwich cores under combined transverse shear and compression. *Composites Part A* 2007; 38: 1288–1295. DOI: 10.1016/j.compositesa.2006.11.008.

25. Petras A and Sutcliffe MPF. Indentation failure analysis of sandwich beams. *Compos Struct* 2000; 50: 311–318. DOI: 10.1016/S0263-8223(00)00122-7